A Simple Synthesis Method for Gold Nano-and Microplate Fabrication Using a Tree-Type Multiple-Amine Head Surfactant

ARTICLE *in* CRYSTAL GROWTH & DESIGN · MARCH 2010

Impact Factor: 4.89 · DOI: 10.1021/cg9008976

4 AUTHORS, INCLUDING:

Guanhua Lin
National University of Singapore
11 PUBLICATIONS **103** CITATIONS

SEE PROFILE

Long Jiang
Chinese Academy of Sciences
128 PUBLICATIONS **1,880** CITATIONS

SEE PROFILE

DOI: 10.1021/cg9008976

CRYSTAL GROWTH & DESIGN Article

2010, Vol. 10
1118–1123

A Simple Synthesis Method for Gold Nano- and Microplate Fabrication Using a Tree-Type Multiple-Amine Head Surfactant

Guanhua Lin, Wensheng Lu, Wenjuan Cui, and Long Jiang*

Beijing National Laboratory for Molecular Sciences, Key Laboratory of Colloids and Surfaces, Institute of Chemistry, Chinese Academy of Sciences, Beijing 100190, People's Republic of China

Received July 30, 2009; Revised Manuscript Received January 7, 2010

ABSTRACT: In this paper, a single tree-type multiple-head surfactant, bis (amidoethyl-carbamoylethyl) octadecylamine (C18N3), which functions as both the reducing and capping agent in the reaction system, has been used to fabricate gold nano- and microplates. The triangle and hexagonal plate, polyhedron, and sphere morphology of the gold nanoparticles could be easily controlled simply by changing the molar ratio of C18N3/$HAuCl_4$. Other influences on the morphology of the gold particles, such as Cl^- concentration, temperature and time, were also studied. At standard conditions, 80 °C, and a molar ratio C18N3/$HAuCl_4$ of 6.9 in a 0.5 M KCl aqueous solution, the size of the plates could be manipulated from several tens of nanometers to several micrometers just by changing the C18N3 concentration. A crystalline growth process for the nanoplate formation has been observed in this system. At the initiation of the crystalline formation, the predominant morphology was triangular, followed by a mixture of triangular, hexagonal, and truncated triangular structures as the particle grew larger. Ultimately, the structures became primarily hexagonal. As-prepared gold nano- and microplates greatly enhanced the surface enhanced Raman scattering (SERS) of ascorbic acid molecules compared to that of other gold nanoparticle morphologies.

Introduction

In recent years, interest in the preparation and characterization of nanostructured materials has continued to grow because of the distinctive properties and potential applications of these materials in nanotechnologies.[1−4] Since the catalytic, optical, biomimic, and electronic properties of nanomaterials depend primarily on their shape and size, one of the desired structural goals is to obtain uniform size and morphology in a controlled manner for metallic and semiconductor materials.[5−7] Gold particles of nanometer or micrometer size and with unique morphologies are particularly attractive materials because of their outstanding properties. Consequently, many published reports have focused on the preparation of various colloidal gold morphologies, including cubes,[8,9] belts,[10] rods and wires,[11−13] disks and plates,[14−17] and urchin-like shapes,[18] among others.

Of the many different shapes of gold particles, gold plates are an especially interesting class of structures because of their unusual shapes and unique optical features.[19] Although many methods have been developed for synthesizing nano- and microplates, only a few systems that produce large, smooth surfaced gold plates have been documented.[20] However, most gold-plate preparation methods are tedious and complicated, do not easily produce monomorphological plates, and cannot be conducted on a large scale. Moreover, the property of nano- and microplates often depends on the method of preparation. Therefore, searching for simpler solutions for the preparation of gold nano- and microplates with controlled diameters is worthwhile.

In the present study, we used a tree-type multiple-amine-group head surfactant (C18N3) synthesized in our laboratory as a template to grow gold nano- and microplates without any requirement for other reductants. This method has the following obvious advantages: (i) the yield of plate morphology under optimal conditions can approach 80% of the population; (ii) there is a very large concentration tolerance for C18N3 in the formation of gold plates (when the concentration of C18N3 changed from 0.1 mM to 2 mM under specific conditions, the morphology still kept the plate form as the size of the gold plates grew from about 20 nm to 15 μm); (iii) no other reducing agent is required, which reduces the influence of the reductant and simplifies the fabrication process; (iv) all processes proceed under mild conditions, as wet chemical processes occurring between 60 and 80 °C; and (v) the morphology of the gold nanocrystal can be easily controlled by adjusting the KCl concentration and molar ratios of C18N3/$HAuCl_4$. We believe that this approach can be extended to the synthesis of other noble metal nano- and microplates.

After being prepared in this manner, the gold nanoplates were measured by surface-enhanced Raman scattering (SERS); a very strong effect was observed that has not been previously seen with other gold crystal morphologies.[21−25] This suggests that these gold nanoplates have a great potential in applications such as SERS measurements. We believe that our synthesis approach shows the unique performance of multiple-amine head surfactants and that it can be extended to other tree-type surfactants.

Experimental Section

Chemicals. Hydrogen tetrachloroaurate(III) trihydrate ($HAuCl_4 \cdot 3H_2O$, 2 wt % solution in water), potassium chloride (KCl, 99%), potassium bromide (KBr, 99%), potassium iodide (KI, 99%), potassium acetate (CH_3COOK, 99%), potassium nitrate (KNO_3, 99%), and sodium chloride (NaCl, 99%) were purchased from Aldrich and used as received. Bis-(amidoethyl-carbamoylethyl) octadecylamine (C18N3) was synthesized as reported in the literature.[26] Ultrapure water (18 MΩ cm) was used for all aqueous preparations.

*Corresponding author. E-mail: jiangl@iccas.ac.cn. Fax: +86 10 82612084.

Published on Web 01/27/2010

Scheme 1. Structure of Bis(amidoethyl-carbamoylethyl) Octadecylamine (C18N3)

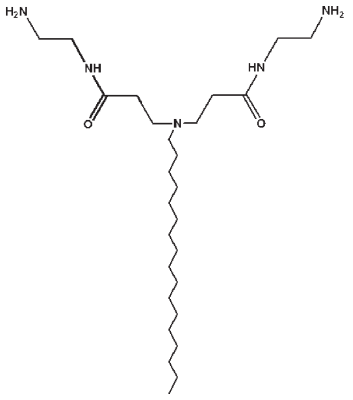

Synthesis of the Multiple Amine Head Surfactant C18N3. The synthesis of C18N3 is a two-step process as reported before[26] and the molecular structure for the C18N3 is shown in Scheme 1.

Synthesis of Gold Microplates. A typical method to fabricate gold microplates was followed. First, 20 mL of potassium chloride solution (0.5 M) was heated with stirring in a three-neck flask to 80 °C over a heating mantle. Then, 5 mL of 10 mM C18N3 aqueous solution was added. One minute later, 1.6 mL of 4.5×10^{-3} M $HAuCl_4$ was added to the flask. To prevent loss of water, the solution was refluxed by connecting one neck of the flask to a condenser, and the others were sealed. The reaction was allowed to proceed for a total of 30 min before the heating mantle was removed from the flask. The solution was kept at room temperature for 24 h, centrifuged at 4500*g*, and washed with water repeated four times. The final products were sandlike golden crystals; the precipitates were redispersed in ethanol for characterization. If the volume of $HAuCl_4$ was reduced to 0.4 and 0.8 mL, the resulting products from this procedure were gold spherical nanoparticles and gold polyhedral gold nanoparticles (decahedron), respectively.

Synthesis of Gold Nanoplates. First, 50 mL of potassium chloride solution (0.5 M) was heated with stirring in a three-neck flask to 100 °C over a heating mantle. Then, 1 mL of 10 mM C18N3 aqueous solution was added. One minute later, 0.32 mL of 4.5×10^{-3} M $HAuCl_4$ was added into the flask, which was sealed and refluxed as already described. The reaction was allowed to proceed for a total of 10 min before the heating mantle was removed from the flask. At this time, the color changed from light yellow to pink. Solvent was removed from the colloid solution by evaporating to a final volume of 10 mL. The sample was centrifuged at 9000*g* and washed four times with ethanol. The precipitates were redispersed in ethanol for characterization.

Characterization. The products were characterized by ultraviolet−visible (UV−vis) spectra (Hitachi U-2800 spectrometer), scanning electron microscopy (SEM, Hitachi S4300, 15 kV), transmission electron microscopy (TEM, JEOL JEM-1011CX, 100 kV), and X-ray diffraction (XRD, Rigaku Dmax-2000, Ni-filtered Cu Kα radiation). For the XRD measurements, the gold product was dispersed in water and several drops of the suspension were dropped onto a clean glass slide, and then left in ambient air to dry. For the TEM and SEM measurements, the suspension was dropped onto a Formvar-covered copper grid and a silicon wafer, respectively, followed by air drying.

Raman measurements were made with a Renishaw System 1000 Raman imaging microscope (Renishaw PLC, U.K) equipped with a 25 mW (1064 nm) He−Ne laser (model 127-25RP, Spectra-Physics, USA) and a Peltier-cooled CCD detector (576 pixels × 384 pixels). A 50× objective (NA = 0.80) mounted on an Olympus BH-2 microscope was used to focus the laser onto a spot approximately 1 μm in diameter and to collect the backscattered light from the sample.

Results and Discussion

In our study, the effects of the $C18N3/HAuCl_4$ molar ratio and C18N3 and KCl concentrations were examined. The effects of aging time and temperature were also studied. As reported by Newman and Blanchard,[27] "many amines are used in AuNP synthesis as both reducing agents and stabilizers, if their reduction potential is of reduction potential between that of the oxidation of Au^0 to Au^{1+} and the reduction potential of $HAuCl_4$ to $Au^{0''}$. Our experiment showed that C18N3 was a candidate amine and no others reductant addition is needed.

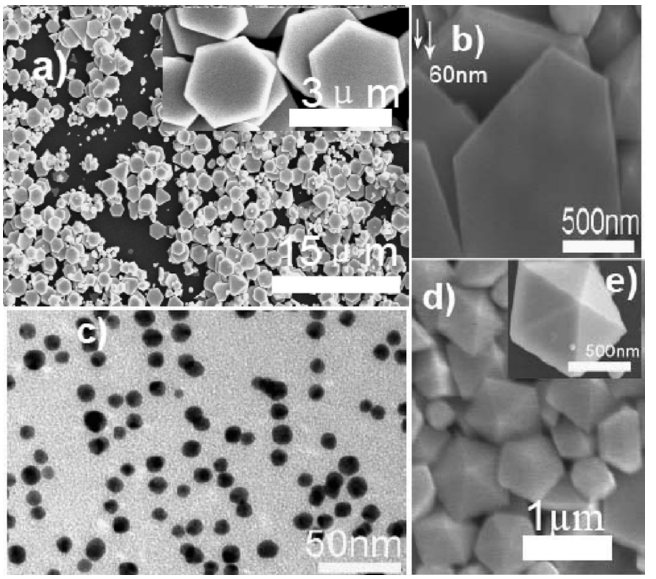

Figure 1. Influence of $C18N3/HAuCl_4$ molar ratios on the morphologies of gold particles. SEM images of various morphologies of gold particles obtained at different molar ratios of $C18N3/HAuCl_4$. (Standard conditions were maintained at 80 °C, 2 mM C18N3 + 0.5 M KCl aqueous solution; for details, see Experimental Section); (a) and (b) show gold microplates prepared at the molar ratio $C18N3/HAuCl_4$ = 6.9; (c) shows gold sphere nanoparticles prepared at the molar ratio $C18N3/HAuCl_4$ = 27.8; (d) and (e) show gold decahedron nanoparticles prepared at the molar ratio C18N3/HAuCl4 = 13.9.

Influence of Molar Ratios of $C18N3/HAuCl_4$ on the Morphologies of Gold Nanoparticles. Figure 1 shows the morphologies of gold particles obtained at different molar ratios of $C18N3/HAuCl_4$. When the molar ratio was larger than 27.8, almost all of the products were spherical gold nanoparticles with a broad size distribution of 20−250 nm, other morphologies of gold nanoparticles were rarely seen. As the molar ratio decreased, the fraction of nanospheres also decreased, and the fraction of decahedrons (edge length 300−600 nm) gradually increased to 50% with the remaining structures appearing as nanospheres and a few nanoplates. If the molar ratio continued to decrease to 6.9, the fraction of gold plates with the triangle and hexagonal shapes increased to about 80%. It is interesting that at this molar ratio, the plate morphology could be kept even if their size increased almost 1000 times. The edge lengths of triangle and hexagonal gold plates were between 800−1600 and 950−2000 nm, respectively. The hexagonal gold plates tended to be larger than the triangle ones. This experiment showed that the molar ratio of $C18N3/HAuCl_4$ plays a predominant role in the morphology of gold nanoparticles.

Figure 1a shows the SEM images of the microplates obtained in an aqueous solution of 2 mM C18N3 + 0.5 M KCl at a molar ratio of $C18N3/HAuCl_4$ = 6.9 for 30 min at 80 °C. The major morphologies of the particles were polygonal plates, including triangle and hexagonal shapes. To

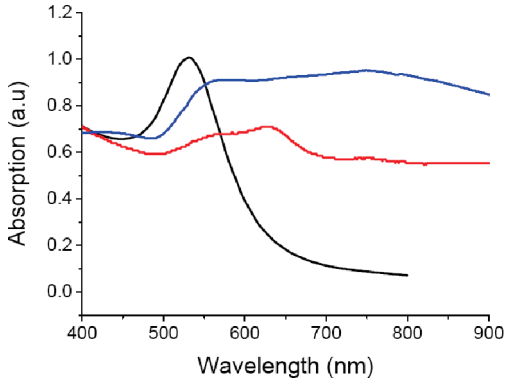

Figure 2. UV−vis absorption spectra of gold particles obtained in solutions with different molar ratios of C18N3/$HAuCl_4$. The black line shows the absorption spectrum of gold nanospheres, the red line shows the absorption spectrum of gold decahedrons, and the blue line shows the absorption spectrum of gold microplates. The molar ratios were 27.7, 13.8, and 6.94, respectively. The reaction temperature was 90 °C.

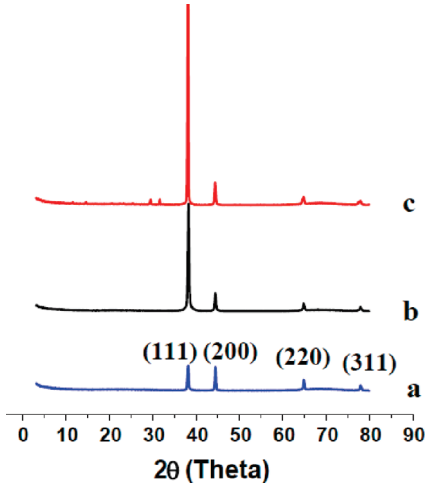

Figure 3. XRD results of different morphology of gold crystals: (a) spheres, (b) decahedrons, (c) plates.

obtain more information about the microplates, the thickness was measured on microplates that were leaning on other gold crystals. As shown in Figure 1a,b, the microplates were about 2 μm in diameter and about 60 nm in thickness.

Gold nanostructures are known to display a very intense color due to their surface plasmon resonance (SPR) and we saw the color clearly on the wall of the flask after the reaction, as the products displayed a very beautiful golden hue. Generally speaking, when major products are spherical gold nanoparticles, a sharp band appears around 550 nm caused by the surface plasmon resonance of gold nanoparticles, and it is usually red-shifted to longer wavelengths with increasing particle size.[28] According to some reports on gold and silver nanoplates, the absorption spectra normally exhibit two or four peaks, because of mutually overlap of different dipole resonances.[29−31]

Variation in the UV−vis absorption spectrum of gold particles with different morphologies shown in Figure 2 was consistent with the results obtained by TEM measurements. When the molar ratio of C18N3/$HAuCl_4$ was 27.8, a sharp absorption band appeared at 537 nm due to the formation of nanospheres. With a decrease in the molar ratio, the adsorption peaks of products became broadened

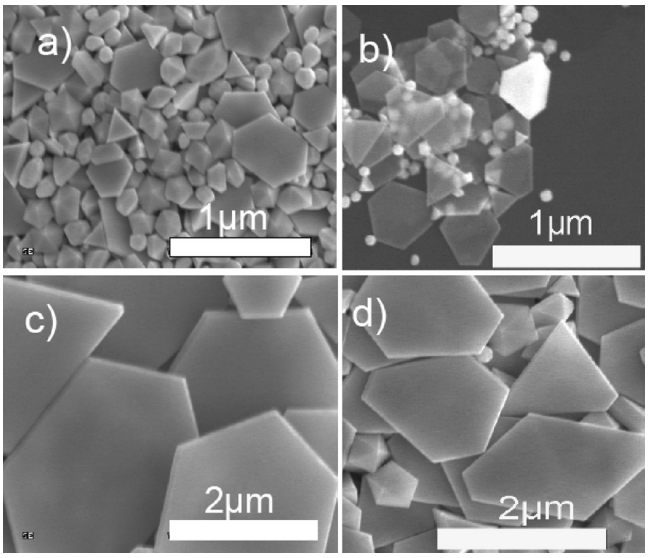

Figure 4. Influence of KCl on the morphology of gold crystals at standard conditions. SEM images of the gold crystals obtained at different KCl concentrations: (a) 0 M, (b) 0.25 M, (c) 0.5 M, (d) 1 M. (Standard conditions of 80 °C, 2 mM C18N3 and a molar ratio C18N3/HAuCl4 = 6.9 were maintained.)

and red-shifted, indicating the formation of gold microplates. The molar ratio of C18N3/$HAuCl_4$ significantly affected the formation of gold crystals, especially gold plates. Various morphologies of gold crystals could clearly be obtained by simply controlling the molar ratio of C18N3/$HAuCl_4$.

Powder XRD analysis gave us further information of the structures of the microplates. As shown in Figure 3, the XRD peaks appeared at (111), (200), (220), and (311), indicating gold with a face-centered cubic (fcc) structure (JCPDS card no. 04-0783). The (111) peak in the gold plate was the strongest among those in these three kinds of gold nanoparticle morphologies.

Effect of KCl Concentration. Many papers have reported that halide ions play an important role in the formation of nanoplates.[32,33] In our reaction system, we found that Cl^- ions greatly increased the size of gold plates, as indicated in Figure 4. When $HAuCl_4$ was reduced in the absence of KCl, the obtained products contained a range of morphologies of gold particles, such as rods, wires, plates, and spheres. As the KCl concentration was increased, the fraction of gold plates increased sharply and the gold rods and wires disappeared. However, with continued increases in KCl concentration, many of the gold plates lost their sharp edges and their forms became eroded. As the KCl concentration approached 1 M, almost all of the gold plates lost their sharp edges, as seen in Figure 4d. We attribute this result to the sculpting effect of chloride ions, which has been reported eleswhere.[34] Therefore, to obtain gold plates at a high yield (about 80%) with sharp edges, the concentration of the KCl was maintained at 0.5 M in our experiments, as shown in Figure 4c.

Influence of C18N3 Concentration. Figure 5 shows SEM and TEM images of gold crystals obtained (80 °C, 0.5 M KCl) at different concentrations of C18N3 (0.1−2 mM) while maintaining the molar ratio of C18N3/$HAuCl_4$ = 6.9. When C18N3 was at 2 mM, the obtained gold nanoplates were about 15 μm in diameter. When the C18N3 concentration decreased to 1 mM and 0.5 mM, the size of the gold plates ranged from about 6 to 1 μm. Further

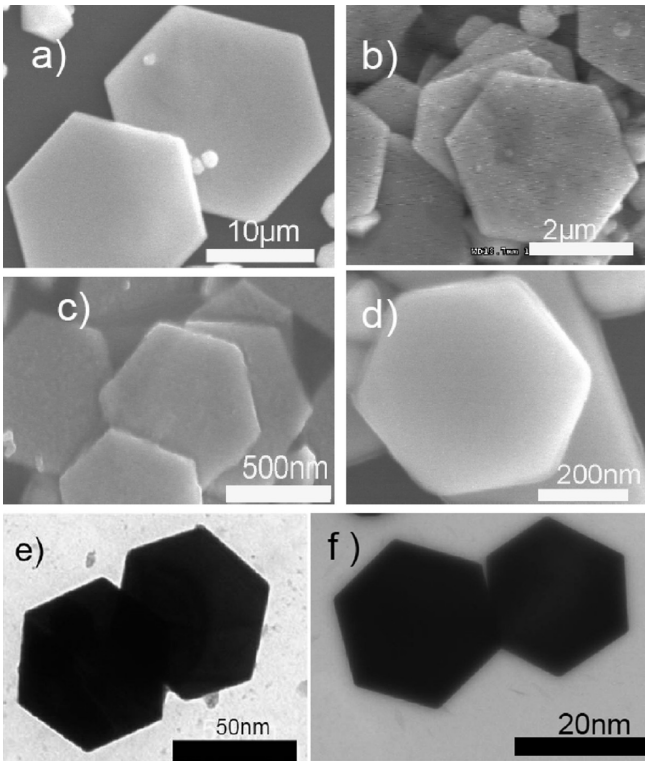

Figure 5. Influence of concentration of C18N3 on the size of gold nanoplates at standard conditions. SEM and TEM images of gold nano- and microplates obtained at different concentrations of C18N3, (a) 2 mM, (b) 1 mM, (c) 0.5 mM, (d) 0.25 mM, (e) 0.125 mM, (f) 0.1 mM. (Standard conditions of 80 °C, 0.5 M KCl and a molar ratio of C18N3/$HAuCl_4$ = 6.9 were maintained.)

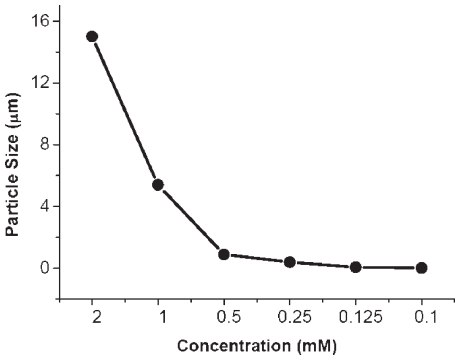

Figure 6. The relationship between the C18N3 concentration and the average size of the gold plates at the standard condition.

decreasing the concentration of C18N3, particularly when the C18N3 concentration reached 0.25 mM, resulted in an increase in the fraction of triangle plates and a decrease in the fraction of hexagonal plates. These results suggest that the triangle plates tended to form at the nanosized level, whereas the size of hexagonal plates could reach 15 μm, as shown in Figure 5a. In other words, gold plates between 20 nm to 15 μm could be successfully fabricated simply by adjusting the C18N3 concentration. Figure 6 shows the relationship between C18N3 concentration and the size of the gold plates.

Effect of Reaction Temperature and Time. Figure 7 shows the SEM images of particles obtained at different reaction temperatures. When the reaction temperature was 60 °C, gold particles formed with sizes at a nanometer scale and with shapes that included triangle and hexagonal plates and

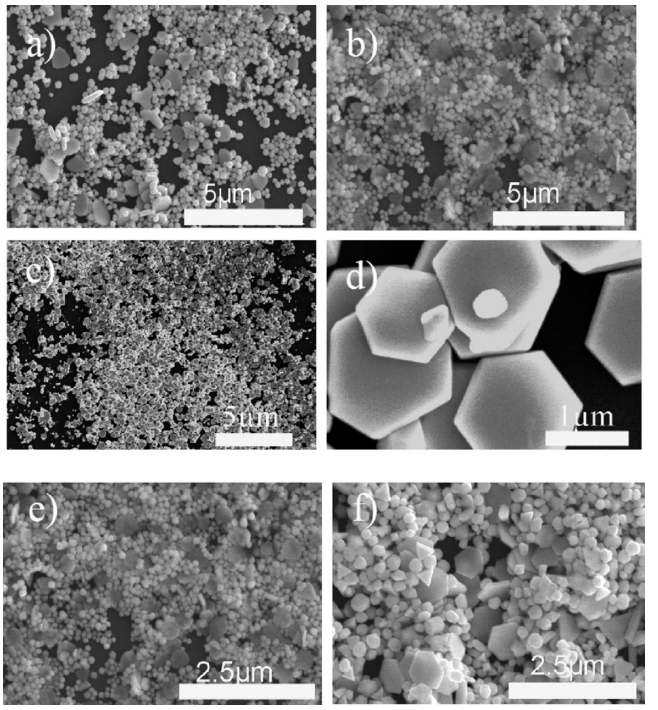

Figure 7. SEM images of particles obtained at different reaction temperatures (Standard conditions of 0.5 M KCl, 2 mM C18N3, and a molar ratio of C18N3/$HAuCl_4$ = 6.9 were maintained): (a) 60 °C, (b) 70 °C, (c, d) 80 °C (high magnification of the gold nanoplates of (c)), (e) 90 °C, (f) 100 °C.

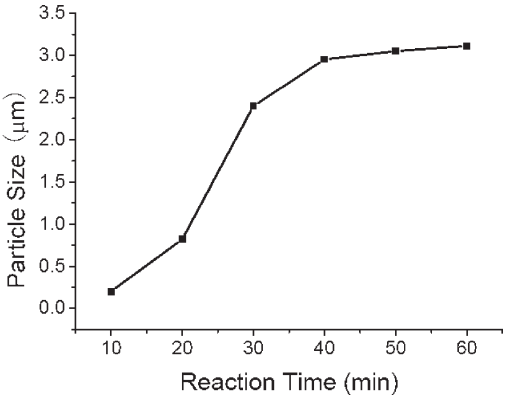

Figure 8. Average particle size at different reaction times (80 °C, 0.5 M KCl, 1 mM C18N3 and molar ratio maintained at C18N3/$HAuCl_4$ = 6.9).

spherical particles. The fraction and the size of the gold plates increased when the temperature was increased from 60 to 80 °C. However, if the reaction temperature was further increased from 80 to 100 °C, the fraction of the gold plates decreased and the size of the gold plates reverted to the nanometer level from the micrometer scale. Therefore, the highest fraction of gold plates could be obtained with a reaction temperature of 80 °C.

Figure 8 shows the average size of gold plates at different reaction times. At reaction times of 20 min and less, the sizes of the gold plates were at the nanometer level. The particle size increased remarkably to the micrometer level within just 30 min. In the early stages of the reaction, the fraction of trihedral plates was high, but these decreased at 30 min and above. Conversely, the fraction of hexagonal plates increased. After 40 min, large gold plates formed and the size

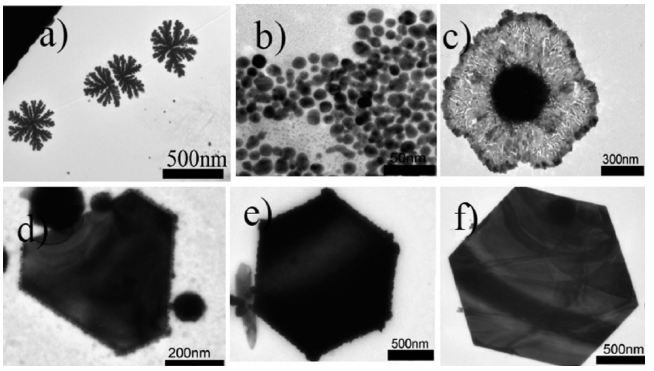

Figure 9. TEM images of the products collected various times after reaction, (a) 30 s, (b) high magnification of the gold nanostructures shown in panel (a), (c) 1.5 min, (d) 5 min, (e) 20 min, and (f) 30 min. The standard reaction condition is 0.5 M KCl, 1 mM C18N3, and a molar ratio of C18N3/$HAuCl_4$ = 6.9 were maintained at 80 °C.

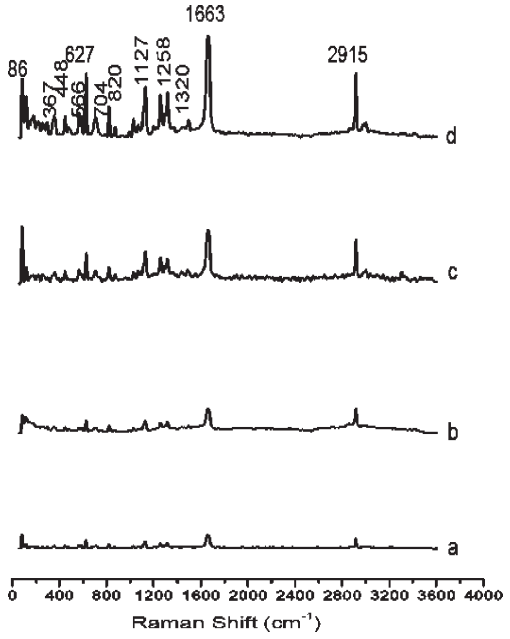

Figure 10. SERS spectra of solid ascorbic acid (a), and ascorbic acid molecules on different gold substrates, (b) gold spherical nanoparticles, (c) gold decahedron nanoparticles, (d) gold nanoplates.

had no significant changes. However, after the reaction had stopped, if the products were left undisturbed for 24 h, the gold plates could continue to grow in size to about 200 nm, and the fraction of gold plates could also increase somewhat. After that, no further changes occurred in the gold plates.

Discussion on the Formation of Gold Plates. Figure 10 shows the dynamic process of gold plates formation. It is interesting that there are two steps involved in the formation of a hexagonal colloid plate crystal; the first is cluster formation and the second is crystal growth. At the beginning of the gold-plate growth process, after the $HAuCl_4$ was mixed with C18N3 solution, intermediate products could be observed. Figure 9a shows the image of these clusters formed after just 30 s of reaction time. Figure 9b is a high magnification TEM image of Figure 9a and shows that the gold nanostructures presented in Figure 9a were composed of irregularly shaped gold nanoparticles about 15 nm in diameter. The extensive formation of these dendritic or radial structures continued to be observed in samples collected after 1.5 min of reaction, as illustrated in Figure 9c. The darker central region appeared to contain a dense assembly of fused gold nanoparticles and formed a large mass several hundreds of nanometers in size.

The reaction proceeded so rapidly that some nanoplates had appeared within a few minutes of the initiation of the reaction. Figure 9d shows a TEM image of a truncated triangle nanoplate with a width of ~400 nm formed after 5 min of reaction. This gold nanoplate seemed to be composed of winding nanowire structures or some type of elongated nanostructures with a size of several nanometers, which were closely arranged to fill the entire nanoplate. We believe that in the case of surfactant available, the gold seeds will form on the active sites in the surfactant aggregates as shown in Figure 9a,b.

Nanoplates with well-defined shapes were formed largely after 20 min of reaction, although some nanoplates had not finished their reaction, as is shown the TEM image in Figure 9e, which shows a hexagonal nanoplate obtained after 20 min of reaction. The edges of the nanoplate still clearly possess rough surfaces, presumably because the exterior nanostructures had not yet completely integrated into this nanoplate. Similar results have also been reported by Huang et. al, who has used sodium citrate to reduce $HAuCl_4$ and CTAB as the capping agent to investigate the growth process of gold nanoplates formed by a thermal aqueous-solution approach.[15] A hexagonal microplate obtained after 30 min of reaction was found to possess the same structurally perfect edges as those shown in Figure 9f.

According to the above results, we can propose a process growth of hexagonal nanoplates in our reaction system. First, leaf-like or elongated winding nanostructures emerged, and these nanostructures very rapidly formed large aggregated structures, within a few seconds after the start of the reaction. These nanostructures with amine heads provided favorite sites for the good seed formation. Next, these leaf-like or elongated winding nanostructures, which tended to be fused more extensively toward the central region, formed a thick mass, and as increasingly more of these nanostructures became integrated, the central core grew in size. Although the gold atoms could be continuously added to the exterior nanostructures in the reaction solution, there was a tendency for the exterior fine structures to decrease in their overall extended sizes relative to that of the central region. After this growth process was completed, the process of gold atom reorganization commenced, yielding final nanoplate products with a well-defined structure.

SERS Measurement. The SERS spectra of the ascorbic acid molecules adsorbed onto the gold nanostructures with different gold crystal morphologies were compared, as shown in Figure 10. The concentration of ascorbic acid was about 4 mg/mL (about 2×10^{-5} M), and 10 mg/mL for the gold materials (i.e., 1×10^{-10}, 2.2×10^{-14}, and 7.5×10^{-13} M for the gold nanocrystalline spherical, plate and decahedron, respectively. See details in Supporting Information). The observed SERS bands that can be assigned to ascorbic acid molecules included ν (C—H) antisymmetric stretching vibration (2915 cm^{-1}), ν (C═O) stretching vibration (1663 cm^{-1}), ν(C═C) stretching vibration (1320 cm^{-1}), ν (C—O) antisymmetric stretching vibration (1258 cm^{-1}), ν (C—O—C) antisymmetric stretching vibration (1127 cm^{-1}), ν (C—O—C) symmetric stretching vibration (819 cm^{-1}), ν (C—C) ring-symmetry-breathing vibration (627 cm^{-1}).[35]

Noticeable changes in the frequency shift and relative intensity of the bands could be observed from the SERS spectra on gold nanoplate substrates, which might have potential applications in the analysis of a variety of organic molecules. A similar result has been reported, stating that the nanoplates of Ag acted as a better SERS support than Ag spheres nanoparticles.[36] As-prepared gold nanoplate appeared to be highly active substrates for the SERS detection of molecule species, a property that most likely originates from their sharp corners and edges of the gold nanoplate. According to the results of XRD measurements shown in Figure 3, we believe the SERS enhancement is closely related with the 111 peak formation on the as-prepared hexagonal plate surface.

Conclusion

In this work, a tree-type multiple-amine head surfactant, which acted as both reducing agent and capping agent in the reaction system, has been used to fabricate gold plates with diameters ranging from several tens of nanometers to several micrometers. Long reaction times and complex procedures were not required to fabricate gold plates, and the size of the gold plates could be well controlled. In addition, nanoparticles consisting of gold decahedrons were obtained by simply adjusting the molar ratio of C18N3/$HAuCl_4$. Both the gold decahedron nanoparticles and the hexagonal gold plates were used as substrate materials for the SERS substrate for detecting the enhanced Raman spectra of ascorbic acid molecules. Both materials, but especially the plate form, showed enhancement of the intensity of the Raman spectra of ascorbic acid molecules.

The growth process of the gold plates has also been addressed in our work. At first, the gold seeds will form on the C18N3 to make a leaf-like template, and then the gold plates were formed by irregular nanostructures that aggregated toward the center to create a fused mass. As the center mass of the polycrystalline gold structure grew in size through continuously incorporating the exterior dendritic gold nanostructures, the gold atoms were reorganized and eventually adopted the plate morphology. However, these kinds of nano- and microplates showed special behavior in the XRD and SERS, indicating a special nano- and microstructure effect existed. We do not know the exact reason behind this effect, and further study is underway. Our study may aid in clarifying the mechanism of gold plate formation and the transformation between the triangular and hexagonal nanoplates. More than that, in the case of C18N3, no other reductants were needed, which simplified the fabrication procedure and provided a new way for the formation of these kinds of particles.

Acknowledgment. This research is supported by the National Natural Science Foundation of China (Grant Nos. 90207026, 90607024, 20903106, 20933007) and Center of Molecular Science of Chinese Academy of Sciences (Grant No. CMS-CX200825).

Supporting Information Available: Calculations for comparing the concentrations of the different morphologies of the gold crystals. This information is available free of charge via the Internet at http://pubs.acs.org/.

References

(1) Lewis, L. N. *Chem. Rev.* **1993**, *93*, 2693–2730.
(2) Mallin, M. P.; Murphy, C. J. *Nano Lett.* **2002**, *2*, 1235–1237.
(3) Park, S. J.; Taton, T. A.; Mirkin, C. A. *Science*. **2002**, *295*, 1503.
(4) Duan, X.; Huang, Y.; Cui, Y.; Wang, J.; Lieber, C. M. *Nature* **2001**, *409*, 66.
(5) Henglein, A. *J. Phys. Chem.* **1993**, *97*, 8457.
(6) Kamat, P. V. *Prog. React. Kinet.* **1994**, *19*, 277.
(7) Hussain, I.; Graham, S.; Wang, Z. X.; Tan, B.; Sherrington, D. C.; Rannard, S. P; Cooper, A. I.; Brust, M. *J. Am. Chem. Soc.* **2005**, *127*, 16398.
(8) Im, S. H.; Lee, Y. T.; Wiley, B.; Xia, Y. *Angew. Chem., Int. Ed.* **2005**, *44*, 2154.
(9) Wiley, B.; Herricks, T.; Sun, Y.; Xia, Y. *Nano Lett.* **2004**, *4*, 1733.
(10) Zhao, N. N.; Wei, Y.; Sun, N. J.; Chen, Q.; Bai, J. W.; Zhou, L. P.; Qin, Y.; Li, M. X.; Qi, L. M. *Langmuir* **2008**, *24*, 991–998.
(11) Mohamed, M. B.; Ismail, K. Z.; Link, S.; EI-Sayed, M. A. *J. Phys. Chem. B* **1998**, *102*, 9370–9374.
(12) Kim, F. K.; Sohn, K. N.; Wu, J. S.; Huang, J. X. *J. Am. Chem. Soc.* **2008**, *130*, 14442–14443.
(13) EI-Sayed, M. A.; Nikoobakht, B. *Chem. Mater.* **2003**, *15*, 1957.
(14) Chen, S.; Carroll, D. L. *Nano Lett.* **2002**, *2*, 1003.
(15) Huang, W. L.; Chen, C. H.; Huang, M. H. *J. Phys. Chem. C*. **2007**, *111*, 2533–2538.
(16) Bai, X. T.; Zheng, L. Q.; Li, N.; Dong, B.; Liu, H. G. *Cryst. Growth Des.* **2008**, *8*, 3840–3846.
(17) Umar, A. A.; Oyama, M.; Salleh, M. M.; Majlis, B. M. *Cryst. Growth Des.* **2009**, *9*, 2835–2840.
(18) Lu, L. H.; Ai, K. L.; Ozaki, Y. K. *Langmuir* **2008**, *24*, 1058–1063.
(19) Millstone, J. E.; Métraux, G. S.; Mirkin, C. A. *Adv. Funct. Mater.* **2006**, *16*, 1209.
(20) Millstone, J. E.; Hurst, S. J.; Métraux, G. S.; Cutler, J. I.; Mirkin, C. A. *Small*. **2009**, *5*, 646.
(21) Fleischmann, M.; Hendra, P.; McQuilan, A. *Chem. Phys. Lett.* **1974**, *6*, 163.
(22) Lu, G.; Li, C.; Shi, G. *Chem. Mater.* **2007**, *19*, 3433.
(23) Wang, T.; Hu, X.; Dong, S. *J. Phys. Chem. B*. **2006**, *110*, 16930.
(24) Orendorff, C. J.; Gole, A.; Sau, T. K.; Murphy, C. *J. Anal. Chem.* **2005**, *77*, 3261.
(25) Alvarez-Puebla, R. A.; Aroca, R. A. *J. Anal. Chem.* **2009**, *81*, 2280–2285.
(26) Wang, W.; Lu, W. S.; Jiang, L. *J. Phys. Chem. B*. **2008**, *112*, 1409–1413.
(27) Newman, J. D. S.; Blanchard, G. J. *Langmuir* **2006**, *22*, 5882.
(28) Jin, R.; Cao, Y. C.; Hao, E.; Metraux, G. S.; Schatz, G. C.; Mirkin, C. A. *Nature* **2003**, *425*, 487.
(29) Maillard, M.; Giorgio, S.; Pileni, M. P. *Adv. Mater.* **2001**, *14*, 1084–1086.
(30) Zhao, Q.; Hou, L.; Zhao, C.; Gu, S.; Huang, R.; Ren, S. *Laser. Phys. Lett.* **2004**, *1*, 115–117.
(31) Lee, J. H.; Kamada, K.; Enomoto, N. Y.; Hojo, J. C. *Cryst. Growth Des.* **2008**, *8*, 2638–2645.
(32) Ha, T. H.; Koo, H. J.; Chung, B. H. *J. Phys. Chem. C* **2007**, *111*, 1123.
(33) Rai, A.; Singh, A.; Ahmad, A.; Sastry, M. *Langmuir* **2006**, *22*, 736.
(34) An, J.; Tang, B.; Zheng, X. L.; Zhou, J.; Dong, F. X.; Xu, S. P.; Wang, Y.; Zhao, B.; Xu, W. Q. *J. Phys. Chem. C* **2008**, *112*, 15176–15182.
(35) Edsall, J. T.; Sagall, E. L. *J. Am. Chem. Soc.* **1943**, *65*, 1312–1316.
(36) Yang, Y.; Matsubara, S.; Xiong, L. M.; Hayakawa, T.; Nogami, M. *J. Phys. Chem. C* **2007**, *111*, 9095–9104.